Anal. Bioanal. Electrochem., Vol. 9, No. 6, 2017, 660-672

Analytical & Bioanalytical Electrochemistry

www.abechem.com

Full Paper

Role of Anodic Passive Potential on the Electrochemical Response of Pure Tantalum in 0.1 M H_2SO_4 Solution

Arash Fattah-alhosseini,[1,*] Saeed Vafaeian,[1] Ali Reza Ansari[1] and Mostafa Khanmohammadi[2]

[1]*Department of Materials Engineering, Bu-Ali Sina University, Hamedan 65178-38695, Iran*
[2]*Department of Welding & Non-destructive Testing Inspection, Shazand Petrochemical Company, Arak, Iran*

*Corresponding Author, Tel.: +988138292505; Fax: +98 813 8257400
E-Mail: a.fattah@basu.ac.ir

Received: 2 March 2017 / Received in revised form: 20 June 2017 / Accepted: 9 July 2017 / Published online: 30 September 2017

Abstract- In this work, the role of anodic passive potential on the passive and electrochemical response of pure Ta in 0.1 M H_2SO_4 solution was studied. Electrochemical impedance spectroscopy (EIS) plots showed that corrosion resistance of the passive film on the pure Ta increased with the increasing of anodic passive potential. In addition, the semiconductive behavior of the passive films formed on pure Ta in 0.1 M H_2SO_4 solution is evaluated by employing Mott–Schottky (M–S) analysis. Although, semiconducting response of pure Ta in 0.1 M H_2SO_4 solution remains the same as n-type, anodic passive potential significantly affect the levels of donor concentrations. Indeed, M–S analysis revealed that less donor densities in passive film due to higher anodic passive potential deteriorated corrosion resistance of the pure Ta. Also, M–S analysis revealed that flat band potential is quite sensitive to anodic passive potential.

Keywords- Pure Ta, H_2SO_4 solution, Passive layer, Anodic passive potential, Mott–Schottky

1. INTRODUCTION

The outstanding properties of tantalum such as its high melting temperature, biocompatibility and refractoriness has caused the growing applications of this alloy over the

last two decades. Tantalum possesses very wide applications in different fields but the most important uses of this strategic metal are in the areas such as manufacturing of capacitors, implants and surgical tools, and equipment in chemical processing [1-3]. The protection of metallic structures against corrosive environments is one of the key factors for development of today's modern industrial processes. The application of high corrosion resistance metals and alloys such as titanium, zirconium, platinum, tantalum and stainless steels is one of the important solutions to achieve a high degree of corrosion protectiveness. From these resistive materials, however, tantalum is an excellent candidate for application in hot acidic media [4, 5].

Although tantalum has a remarkable passivation tendency in many aggressive environments, this metal can be attacked in some media. Hydrofluoric (HF) acid, fluoride ions in acidic medium, and hot strong alkalis are among the most detrimental and harmful cases that reduce the resistance of tantalum [6-8]. Owing to high price of tantalum, it is not economic to construct the entire part of the construction out of tantalum. Hence, in practice, the equipment is constructed from traditional materials such as stainless steels, and then a thin layer of tantalum is coated on the surface to provide a suitable protectiveness against the aggressive medium. Such a contrivance results in the final product will benefit from both the properties of stainless steel as a cost effective and workable substrate and the advantages of coated tantalum on the surface.

The excellent corrosion resistance of tantalum and its alloys in acidic media are revealed by many researchers. The investigation by Robin et al [2] showed that in boiling sulfuric acid the Nb-Ta alloys is inactive up to 40 wt. % H_2SO_4. In addition, the studies by Kouril et. al. [3] and Nikiforov et. al. [4] on the corrosion behavior of tantalum in 85 wt.% H_3PO_4 indicated that tantalum had a good stability at high temperature. Considering the investigations have been done on the corrosion behavior of tantalum [9-14], it is found that the electrochemical behavior of this alloy in acidic media is less studied. Thus, the main purpose of this research is to evaluate the passive behavior of Ta in H_2SO_4 medium from electrochemical viewpoint by potentiodynamic polarization (PDP), EIS and M–S analysis.

2. EXPERIMENTAL PROCEDURES

All pure Ta specimens were ground to 1200 grit and cleaned with deionized water prior to the tests. The exact details of three-electrode flat cell and electrochemical (PDP, EIS and M–S analysis) measurements were published elsewhere [15]. To evaluate the role of anodic passive potential on the passive and electrochemical response of pure Ta in 0.1 M H_2SO_4 solution at 25±1 °C, we chose four potentials (0.1, 0.3, 0.5 and 0.7 $V_{Ag/AgCl}$) within the passive region to do the survey for potentiostatic film growth, EIS, and M–S tests. Time duration for film growth was considered 1800 s to make sure that the steady-state condition is

on. To provide the EIS data with the appropriate fitted curves, NOVA 2.0.1 impedance software was applied.

3. RESULTS AND DISCUSSION

3.1. Open circuit potential (OCP) and polarization measurements

The OCP curve of pure Ta in 0.1 M H_2SO_4 solution is shown in Fig. 1(a). At the start of immersion, the open circuit potential is directed towards positive values. This trend is also reported for pure Ta in alkaline solutions, which indicates the formation of passive film and its role in increasing protectivity with time. The OPC curves show that within 1200 s a complete stable condition is achieved to implement the electrochemical tests. Fig. 1(b) depicts the PDP plot of pure Ta in 0.1 M H_2SO_4 solution. From the PDP plot, the passive range was determined to be from -0.1 to 1.5 $V_{Ag/AgCl}$.

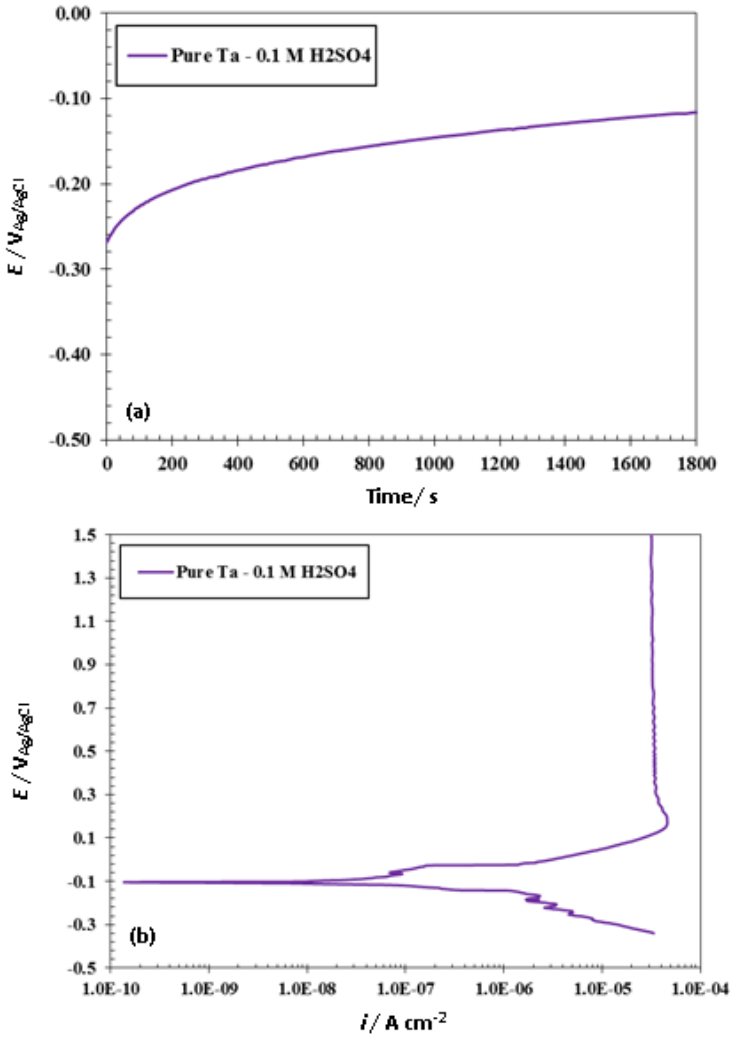

Fig. 1. (a) OCP and (b) PDP plot of pure Ta sample in 0.1 M H_2SO_4 solution

The passive behavior of pure Ta electrode is in agreement with reported literatures [15]. The passive current density appears to be nearly constant just below the breakdown potential. Through formation of the passive layers, the progress of current density was measured during the application of different potentials in the passive region. Fig. 2(a) shows the potentiostatic polarization graphs for pure Ta in 0.1 M H_2SO_4 solution. It is seen that the current density weakens with time until a steady state is established. Fig. 2(b) depicts the rates of the steady-state passive current density (i_{ss}) versus the formation potential. The mean steady-state current density is 2.16 0^{-7} A cm^{-2}.

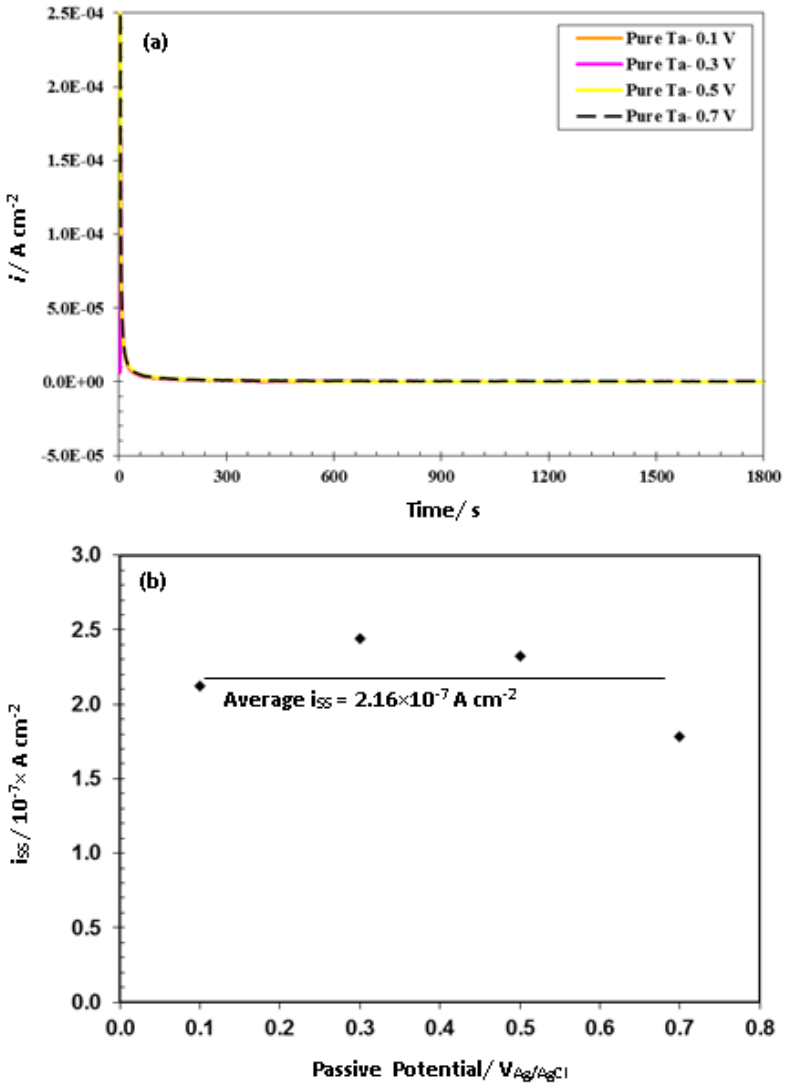

Fig. 2. (a) Potentiostatic polarization plots of pure Ta in 0.1 M H_2SO_4 solution, and (b) steady-state passive current density obtained during the potentiostatic growth of the passive layers

3.2. EIS measurements

Fig. 3 reveals the role of anodic passive potential on the EIS plots of pure Ta in 0.1 M H_2SO_4 solution. For all passive potential, just one capacitive loop is seen (Fig. 3(a)).

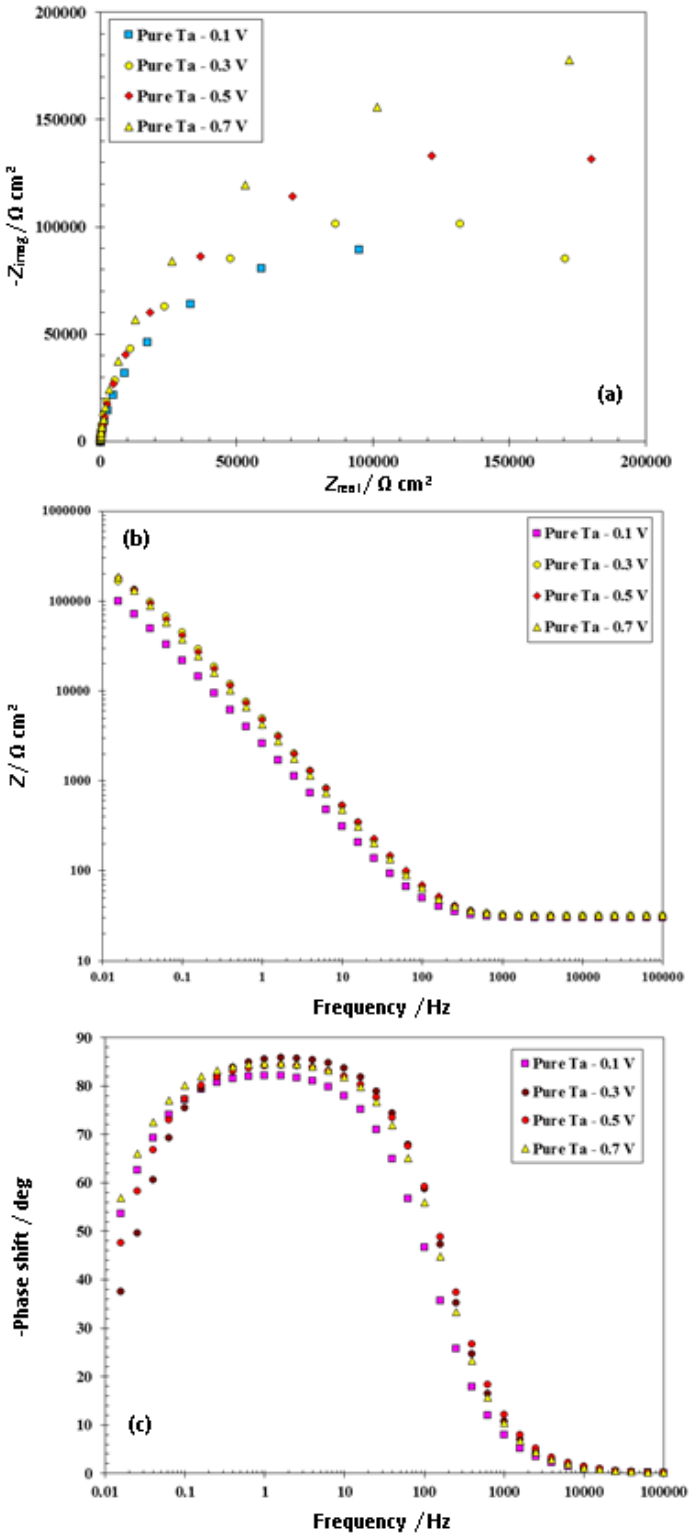

Fig. 3. Role of passive potential on the (a) Nyquist, (b) Bode, and (c) Bode-phase plots of pure Ta in 0.1 M H_2SO_4 solution

It is established that the diameters of these imperfect depressed semicircles are proportional to the resistance of passive films such that any growth in diameter shows an increase in the stability and compactness of the passive layer [16,17]. Also, any increase in the passive potential results in a noticeable increase in the total resistance. Taking into account Bode plots (Fig. 3(b)), one time constant seems to exist. As shown in the Bode-phase plots (Fig. 3(c)), the peak of the phase angle is called to be lower than -90° which is ascribed as an evidence of such behaviors can be interpreted as a deviance from an ideal capacitor. To account for deviation from ideal state, raised through parameters like surface heterogeneity and roughness, a constant phase angle element (*Q*) will be taken into account. *Q* is expressed as follows [17,18]:

$$Q = Y_0 (j\omega)^n \tag{1}$$

Here, Y_0 shows the admittance (Ω^{-1} cm^{-2} s^{-1}), ω is the angular frequency (rad s^{-1}), *j* reveals the imaginary unit, and *n* presents the *Q* exponent varies between 0 and 1 [17,18]. The capacitance of the constant phase element can be calculated from Eq. (2) [17,18]:

$$C = Y_0 (\omega_{max})^{n-1} \tag{2}$$

Here, ω_{max} shows the angular frequency at which the maximum in the imaginary component of the impedance occurs. To simulate the EIS data, the equivalent electrical circuit revealed in Fig. 4 was used. In the equivalent circuit, applied to describe the passive layers formed on Ta and Ti in 0.5 M H_2SO_4 solution [19], the elements of the circuit are defined as: R_s shows the solution resistance, R_p presents the resistance of the passive layer, and Q_p is constant phase element relating to the capacitance of the passive layer.

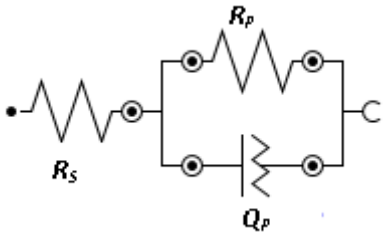

Fig. 4. The Randles circuit for the modeling experimental EIS data [19]

Fig. 5 shows the effect of anodic passive potential on the resistance and capacitance of the passive layers of pure Ta in 0.1 M H_2SO_4 solution.

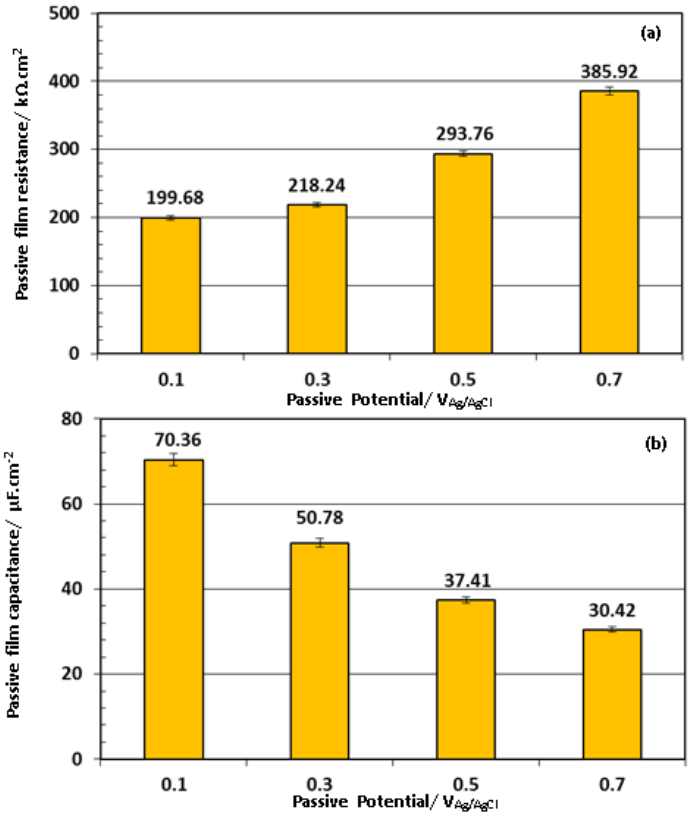

Fig. 5. Effect of passive potential on the (a) passive film resistance and (b) passive film capacitance of pure Ta in 0.1 M H_2SO_4 solution

It is shown that the resistance of the passive layer increases by anodic passive potential (Fig. 5(a)). Also, noting the Fig. 5(b), it is seen that by increasing the anodic passive potential, the passive film capacitance decreases.

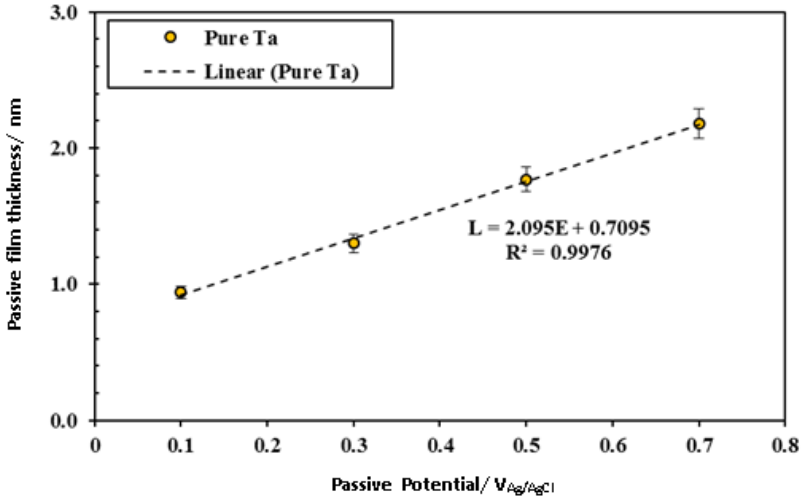

Fig. 6. Role of passive potential on the calculated passive film thickness of pure Ta in 0.1 M H_2SO_4 solution

Such drop in the passive film capacitance implies lower dissolution and the passivity increase [15,17]. Eq. (3) is used to determine the thickness of the passive layer (L) [20,21]:

$$L = \frac{\varepsilon \varepsilon_0 A}{C} \tag{3}$$

Here, ε is the dielectric constant of passive layer (25 for Ta [15,17,20]), ε_0 shows the vacuum permittivity, and A is the effective surface area. Fig. 6 depicts the effect of anodic passive potential on the passive layer thickness of pure Ta in 0.1 M H_2SO_4 solution. The calculated passive layer thickness is in the range of 0.9-2.1 nm, which is agreement with those reported in the literature for pure Ta [22]. Therefore, increasing the passive potential is appropriate to form thicker and more protective passive films for pure Ta in 0.1 M H_2SO_4 solution.

3.3. M–S analysis

Fig. 7 shows the role of anodic passive potential on the M–S plots of pure Ta in 0.1 M H_2SO_4 solution. It can be deduced when the passive potential is 0.1 $V_{Ag/AgCl}$, the space charge capacitance (C_{sc}) possesses the largest magnitude.

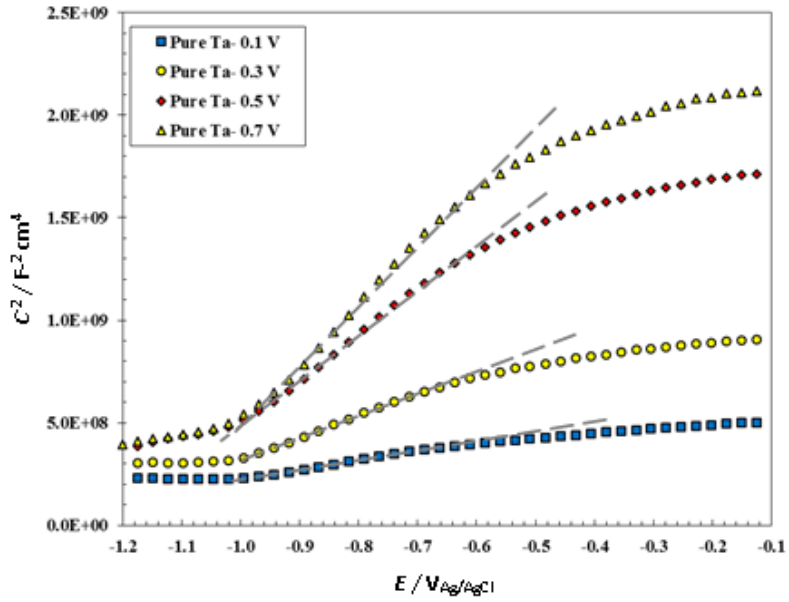

Fig. 7. Role of passive potential on the M–S plots of pure Ta in 0.1 M H_2SO_4 solution

Positive slopes are indicators of n-type semiconducting behavior [23,24]. From these positive slopes using M–S equation, donor densities (N_D) can be expressed as [24,25]:

$$\frac{1}{C_{SC}^{\ 2}} = \frac{2}{\varepsilon \varepsilon_o e N_D}\left(E - E_{fb} - \frac{k_B T}{e}\right) \tag{4}$$

Here *e* is the electron charge, *k* shows the Boltzmann constant, *T* is the absolute temperature, and E_{fb} reveals the flat band potential. By extrapolating linear portion to C_{sc}^{-2}=0, one can determine the flat band potential. It is interesting to note that E_{fb} decreases as the anodic passive potential increase. Revealing in Fig. 8, the defect structure of the passive film formed on pure Ta is pictured through a chain of creation and annihilation of defects that occurs at the interface of metal/passive layer as well as at the interface of passive layer/ solution [15, 26]. A newly developed PDM offers incorporation of oxygen vacancies along with other defects [15].

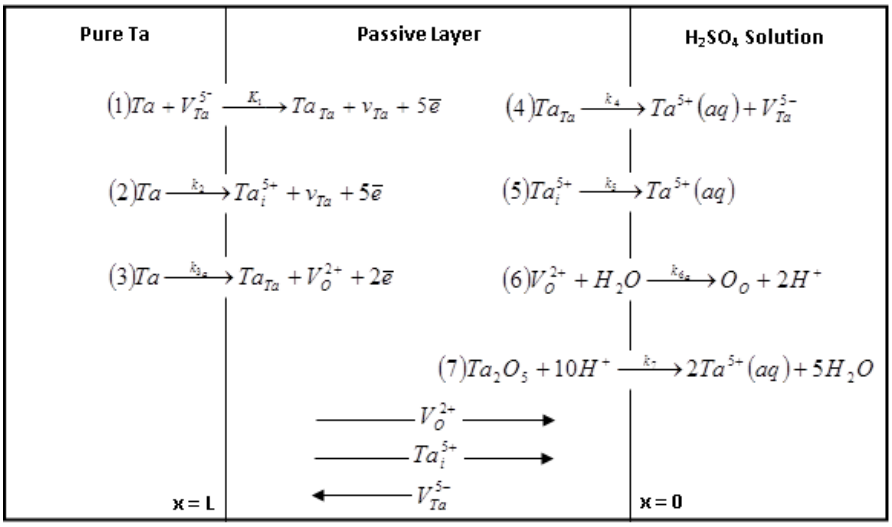

Fig. 8. The modified PDM for passivation of Ta in 0.1 M H_2SO_4 solution. V_{Ta}^{5-}=Ta vacancy on the Ta sublattice of the passive layer, Ta_i^{5+}=interstitial Ta, Ta_{Ta}=Ta cation on the Ta sublattice of the passive layer, V_O^{2+}=oxygen vacancy on the oxygen sublattice of the passive layer, O_O=oxygen anion on the oxygen sublattice of the passive layer, $Ta^{5+}(aq)$=Ta cation in solution

Generally, the flux of cation interstitials and/or oxygen vacancies through the passive film are needed for the growth process of the film. Anodic passive potential contribute significantly to the formation of point defects. Therefore, the relative dominance of kinetics of reaction (3) with respect to the kinetics of reaction (7) may hold accountable for the downward trend of thickness values at the said H_2SO_4 concentration. The *n*-type electronic behavior of the passive layer cannot be justified since the cation vacancies are electron acceptors. Thus, it can be concluded that the governing defects in the passive layer are possibly oxygen vacancies acting as electron donors; by this mean, the passive layer is doped *n*-type as mentioned earlier in the M–S plots. For all M–S plots (Fig. 7), two linear-like regions seems to exist in the range of -1.0 $V_{Ag/AgCl}$ to -0.1 $V_{Ag/AgCl}$. Some literatures justify these multiple slopes differently [15,17]. Some hypotheses include the presence of surface

states, change in donor type, inhomogeneous donor distribution, as well as the presence of a second donor level in the band gap, which is supposed to be an outcome of partial ionization of deep donors [27, 28]. Fig. 9 depicts the effect of anodic passive potential on the calculated donor densities of pure Ta in 0.1 M H_2SO_4 solution.

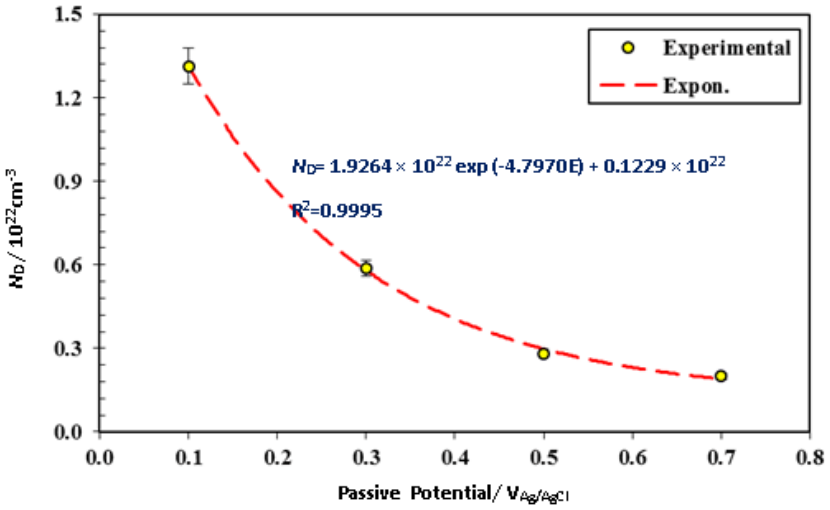

Fig. 9. Role of anodic passive potential on the calculated donor density of the passive layers formed on pure Ta in 0.1 M H_2SO_4 solution

The donor densities are in the order of magnitude of 10^{22} cm^{-3}; this is corresponding to those reported previously [15,17,29]. High values of the donor densities may correspond with higher density of oxygen vacancies in the passive layer [15,17,29]. Donor density reaches its minimum values when the passive potential is 0.7 $V_{Ag/AgCl}$. To assess the relationship between donor density and the film formation potential, Eq. (5) was developed [30–33]:

$$N_D = \omega_1 \exp\left(bE_{ff}\right) + \omega_2 \tag{5}$$

Here, ω_1, ω_2 and b are unknown constants determined according to the experimental data. Through nonlinear fitting of the experimental findings, the exponential relationship between the donor density and the formation potential is obtained as Eq. (6) [30,31]:

$$N_D = 1.9264\times10^{22} \exp\left(-4.7970E_{ff}\right) + 0.1229\times10^{22}\left(cm^{-3}\right) \tag{6}$$

Eq. (7) expresses the calculation of the diffusion [30,31]:

$$D_O = -\frac{i_{ss}RT}{4eF\omega_2\varepsilon_L} \tag{7}$$

Here, R and F show the ideal gas constant and the Faraday constant. By substituting i_{ss}, ε_L, and ω_2 into Eq. (7), one can find D_0=7.38±0.15×10^{-18}. Thus, the diffusion coefficient of

defects in the passive film formed on pure Ta in 0.1 M H_2SO_4 solution is estimated in the range of 10^{-18} cm^2/s. This is in the order of the results recorded for defects diffusion coefficient in the passive film for Ta in 0.1 M KOH [34] and 0.1 M H_2SO_4 [35].

4. CONCLUSIONS

In the present study, the role of anodic passive potential on the passive and electrochemical response of pure Ta in 0.1 M H_2SO_4 solution was evaluated. The main findings and conclusions are as follows:

- PDP curve showed that pure Ta sample displays a wide passive range in 0.1 M H_2SO_4 solution.
- Potentiostatic polarization results depicted that the steady-state current density through the passive film of pure Ta sample was independent of formation potential, which is in good agreement with the postulation of the PDM.
- Based on the M–S plots, with increase in the anodic formation potential, the calculated donor density decreases exponentially.
- Linear increase in the thickness of the passive film is observed with the anodic formation potential.
- Considering that the donors are defects including cation interstitials and oxygen vacancies, the experimental data were justified in terms of the PDM for the passivity of pure Ta in 0.1 M H_2SO_4. The calculated diffusivity of defect was in the range of 10^{-18} cm^2/s.

REFERENCES

[1] E. Hosseini, and M. Kazeminezhad, Int. J. Refract. Met. Hard Mater. 27 (2009) 605.

[2] M. Bischof, S. Mayer, H. Leitner, H. Clemens, P. Staron, and E. Geiger, Int. J. Refract. Met. Hard Mater. 24 (2006) 437.

[3] M. D. Bermúdez, F. J. Carrión, G. Martínez-Nicolás, and R. López, Wear 258 (2005) 693.

[4] M. Kouřil, E. Christensen, S. Eriksen, and B. Gillesberg, Mater. Corros. 63 (2012) 310.

[5] A. Robin, and J. L. Rosa, Int. J. Refract. Met. Hard Mater. 18 (2000) 13.

[6] A. V. Nikiforov, I. M. Petrushina, E. Christensen, A. L. Tomás-García, and N. J. Bjerrum, Int. J. Hydrogen Energy. 36 (2011) 111.

[7] S. M. Cardonne, P. Kumar, C. A. Michaluk, and H. D. Schwartz, Int. J. Refract. Met. Hard Mater. 13 (1995) 187.

[8] P. Patnaik, ed. Handbook of Inorganic Chemicals, McGraw-Hill Companies: New York (2003).

[9] A.H. Ramezani, M.R. Hantehezadeh, M. Ghoranneviss, E. Darabi, Appl. Phys. A 122 (2016) 1.

[10] H. Koivuluoto, J. Näkki, and P. Vuoristo, J. Therm. Spray Technol. 18 (2009) 75.
[11] A. C. Manea, M. Buda, and T. Visan, UPB Sci. Bull. B 72 (2010) 65.
[12] C. Friedrich, P. Kritzer, N. Boukis, G. Franz, and E. Dinjus, J. Mater. Sci. 34 (1999) 3137.
[13] G. A. Bukatova, E. G. Polyakov, L. P. Polyakova, and O. Forsen, J. Aromaa, Prot. Met. 36(5) (2000) 456.
[14] K. A. de Souza, and A. Robin, Mater. Chem. Phys. 103 (2007) 351.
[15] A. Fattah-alhosseini, F. R. Attarzadeh, S. Vafaeian, M. Haghshenas, and M. K. Keshavarz, Int. J. Refract. Met. Hard Mater. 64 (2017) 168.
[16] A. Fattah-Alhosseini, and O. Imantalab, Metall. Mater. Trans. A 47 (2016) 572.
[17] F. R. Attarzadeh, N. Attarzadeh, S. Vafaeian, and A. Fattah-alhosseini, J. Mater. Eng. Perform. 25 (2016) 4199.
[18] B. Hirschorn, M. E. Orazem, B. Tribollet, V. Vivier, I. Frateur, and M. Musiani, Electrochim. Acta 55 (2010) 6218.
[19] W. A. Badawy, S. S. Elegamy, and K. M. Ismail, Br. Corros. J. 28 (2013) 133.
[20] J. Xu, W. Hu, S. Xu, P. Munroe, and Z. H. Xie, ACS Biomater. Sci. Eng. 2 (2016) 73.
[21] W. Wang, F. Mohammadi, and A. Alfantazi, Corros. Sci. 57 (2012) 11.
[22] J. W. Schultze, M. Pilaski, M. M. Lohrengel, and U. Konig, Single, Faraday Discuss. 121 (2002) 211.
[23] E. Sikora, J. Sikora, and D. D. Macdonald, Electrochim. Acta 41 (1996) 783.
[24] V. Macagno, And J. W. Schultze, J. Electroanal. Chem. 180 (1984) 157.
[25] W. J. Chun, A. Ishikawa, H. Fujisawa, T. Takata, J. N. Kondo, and M. Hara, J. Phys. Chem. B. 107 (2003) 1798.
[26] J. D. Sloppy, anodization mechanism and properties of bi-layer tantalum oxide formed in phosphoric acid, PhD thesis, The Pennsylvania State University, USA (2009).
[27] L. Hamadou, L. Aïnouche, A. Kadri, S. A. A. Yahia, and N. Benbrahim, Electrochim. Acta. 113 (2013) 99.
[28] M. Khanuja, H. Sharma, B. R. Mehta, and S. M. Shivaprasad, J. Electron Spectros. Relat. Phenomena. 169 (2009) 41.
[29] R. M. Fleming, D. V. Lang, C. D. W. Jones, M. L. Steigerwald, D. W. Murphy, and G. B. Alers, J. Appl. Phys. 88 (2000) 850.
[30] E. Sikora, J. Sikora, and D. D. Macdonald, Electrochim. Acta 4 (1996) 783.
[31] A. Fattah-alhosseini, Arab. J. Chem. 9 (2016) S1342.
[32] J. Liu, and D. D. Macdonald, J. Electrochem. Soc. 148 (2001) B425.
[33] S. Z. Smialowska, and W. Kozlowski, Passivity of Metals and Semiconductors, Netherlands (1983).
[34] R. Cabrera-Sierra, J. Manuel Hallen, J. Vazquez-Arena, G. Vázquez, and I. González, J. Electroanal. Chem. 638 (2010) 51.

[35] R. Cabrera-Sierra, J. Vazquez-Arenas, S. Cardoso, R. M. Luna-Sánchez, M. A. Trejo, J. Marín-Cruz, and J. M. Hallen, Electrochim. Acta 56 (2011) 8040.